Proceedings of the 9th U.S. National and 10th Canadian Conference on Earthquake Engineering
Compte Rendu de la 9ième Conférence Nationale Américaine et
10ième Conférence Canadienne de Génie Parasismique
July 25-29, 2010, Toronto, Ontario, Canada • Paper No 831

CONSTITUTUIVE MODEL FOR BUCKLING OF TRANSVERSALLY RESTRAINED LONGITUDINAL BARS IN REINFORCED CONCRETE COLUMNS

Mohamed M. Talaat[1] and Khalid M. Mosalam[2]

ABSTRACT

This paper introduces a constitutive material model of reinforcing steel bars in reinforced concrete (RC) columns. The model accounts for the restraining effect of transverse reinforcement on the bar buckling length and the stress at the onset of buckling. Once the bar buckles, the material model uses a strain decomposition approach to condense the bar rotational and transversal degrees of freedom and model the post-buckling softening behavior in terms of convenient axial stress and strain quantities. The model incorporates stiffness reduction upon strain reversal from a compression cycle in which bar buckling occurred, and a plastic strain-dependent damage index calibrated to impose hysteretic stress reduction and predict bar fracture. Due to the strain decomposition approach used, the bar buckling model has the advantage of flexibility to use an existing library of steel uniaxial material models as base. The model-predicted monotonic and cyclic axial responses of individual reinforcing steel bars compare well with published experiments. Finally, the proposed model is used successfully to model buckling in the longitudinal reinforcement of two RC bridge column models experimentally tested under combined axial and lateral loading.

Introduction

Reinforcing steel bars generally follow a linear-elastic response in tension up to a yielding strain. Then, nonlinear behavior characterized by elongation with little corresponding change in stress is typically observed, followed by hardening up to an ultimate stress, which is followed by softening and, eventually, fracture. In compression, however, geometric effects, i.e. bar slenderness (length to diameter ratio), usually lead to buckling of the bar before the ultimate stress. Elastic buckling can occur prior to yielding in the more slender bars, while inelastic buckling is observed for less slender bars. After buckling, bars exhibit a softening response with increased compressive strains, since the bar cross-sections in this regime are loaded eccentrically and compressive yielding occurs only on one side of the cross-section while the opposite side of the cross-section is subjected to tension. Many analytical models have been proposed in the literature, which vary in accuracy and complexity, from bilinear to multi-regime nonlinear for unbuckled bar behavior.

[1] Senior Engineer, Simpson Gumpertz & Heger Inc, 1 Market Plaza, San Francisco, CA 94105, mtalaat@sgh.com.
[2] Professor and Vice Chair, 733 Davis Hall, Department of Civil and Environmental Engineering, University of California, Berkeley, CA 94720, mosalam@ce.berkeley.edu.

Buckling of longitudinal bars in compression is a geometric nonlinearity effect which causes the response to deviate from the theoretical (tensile) stress-strain law. As such, its accurate modeling is subject to an accurate balance of geometric and material stiffnesses. Analytical models for steel bar inelastic behavior which include explicitly nonlinear functions more accurately estimate a bar stiffness along the loading history than simple multi-linear models. This study uses the cyclic stress-strain model by (Menegotto and Pinto 1973), complemented by the work of (Chang and Mander 1994) for a better representation of the nonlinear monotonic behavior and the yield plateau.

Experimental investigations were conducted on individual reinforcing bars by several researchers including (Monti and Nuti 1992), (Rodriguez et al. 1999), (Bayrak and Sheikh 2001), and (Dhakal and Maekawa 2002b). These experiments established monotonic and cyclic response data for bars with different strengths, slenderness ratios, and axial load eccentricities. These data led to a number of analytical models to predict the onset of bar buckling and describe post-buckling behavior. Several models, e.g. Rodriguez et al. (1999) assumes that the buckling length is known a-priori and equal to the transverse tie spacing. Experimental observations from RC column tests demonstrate that bar buckling can occur over multiple transverse tie spacings. Therefore, a variable buckling length as well as the lateral restraining effect of these ties should be explicitly considered in predicting the buckling load. The study in (Dhakal and Maekawa 2002a) explicitly considers the buckling of a bar laterally supported by discrete springs representing individual ties. This necessitates the use of iterative procedures to determine the critical number of ties and the corresponding critical stress, which is computationally demanding. Contrastingly, (Berry and Eberhard 2005) proposes a regression-based empirical expression for RC column lateral drift ratio at the onset of bar buckling for a given axial load level. The statistical analysis included in (Berry and Eberhard 2005) employs results from 40 tests of flexure-critical RC columns and results in a fit with 28% coefficient of variation.

The post-buckling behavior of steel bars has been modeled based on one of two approaches. The first approach describes the behavior based on the average strain in the neighboring concrete. In this case, the material model is in effect a structural model of the reinforcing bar, and the model parameters need to be calibrated for the bar geometry. Justification for this average strain approach is presented in (Bayrak and Sheikh 2001), arguing that while the buckled bar loses its bond with the neighboring concrete, the assumption of equal average strain can be maintained at transverse tie locations at the ends of a buckled bar. Other published research works which follow the average strain approach include (Monti and Nuti 1992), (Gomes and Appleton 1997), and (Attolico et al. 2000). The second approach deals directly with large-deformation strains and explicitly models non-uniform stress in the bar cross-section. For example, (Dhakal and Maekawa 2002a, b) use a micro-analytical approach to determine the monotonic softening behavior of buckled bars using solid modeling. Based on simulations for a variety of bar geometry and strength configurations, this softening relationship is then parameterized using average strain quantities and included in a finite element (FE) code. These models use the stress-strain model in (Menegotto and Pinto 1973) as a starting point.

The proposed constitutive model is composed of several components: the idealization of the bar and tie geometry into a uniaxial material framework; the estimation of critical buckling stress and corresponding buckling length; the prediction of monotonic post-buckling behavior using a strain decomposition; the prediction of cyclic behavior and reduced unloading stiffness of buckled bars; and hysteretic stress reduction, modeled as a low-cycle fatigue phenomenon.

Geometric Setup of Laterally-Restrained Longitudinal Bar

The geometric setup and free-body diagram of the buckling-prone longitudinal steel bar encased within a RC column is shown in Fig.1, idealized as a beam-column element supported on uniformly distributed springs. An energy-minimization approach is then used to determine the buckling length and the corresponding critical stress. It is assumed that buckling takes place in the perpendicular direction away from the column core in a bar of diameter d_b over a buckling length L_b spanning more than one transverse tie spacing s_t, of effective stiffness α_t for each tie, that the concrete cover spalls prior to bar buckling and has no restraining effect, and that the bar rotation is restrained at the beginning and end of the buckling length. The figure shows the free-body diagram of the buckled bar at equilibrium in a deformed configuration with buckling-induced lateral displacement δ_n at mid-height. This results in bending moments as shown, in addition to the axial load P satisfying equilibrium. The variation of P along the buckling length is ignored because in the relevant case of post-yield buckling within a plastic hinge region, the stress along the bar in this region is nearly constant. The inclusion of this variation in the formulation requires an iterative solution of the critical buckling length instead of the closed-form analytical expression derived later in Eq. (8). The lateral displacement $y(x)$ along the reinforcing bar is assumed to follow an infinite series of harmonic shape function,

$$y(x) = \sum_{n=1}^{\infty} (\delta_n/2)[1 - \cos(2\pi nx/L_b)]$$ (1)

Moreover, the bar is assumed to have initial imperfection (deformed shape). A formula similar to Eq. (1) describes the initial deformed shape, with lateral displacement δ_i at mid-height.
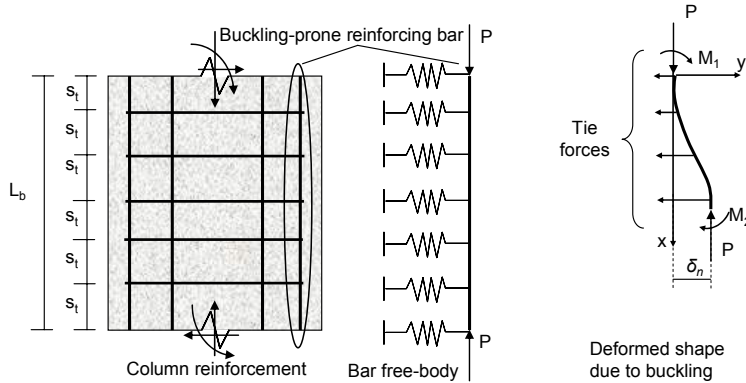
Figure 1. Geometry and free-body diagram of buckling-prone longitudinal bar

Detecting the Onset of Buckling

The elastic strain energy stored in the system due to the increase in axial load on the bar can be evaluated by algebraically adding the contributions from two terms. The first term is derived from the bending moment $M(x)$ and curvature $\phi(x)$ along the buckling length L_b, where $M(x) = E_s J_b \phi(x)$, E_s is the bar elastic modulus, J_b is the bar cross-section moment of inertia, and $\phi(x)$ is the second derivative of Eq. (1). The first term in the strain energy equation can be evaluated by making use of the orthogonality characteristic of trigonometric integrals as

$$\Delta U_{bar} = \frac{1}{2}\int_0^{L_b} M\phi\,dx = \frac{E_s J_b}{2}\int_0^{L_b}\left(\frac{\partial^2 y}{\partial x^2}\right)^2 dx = \frac{E_s J_b}{2}\sum_{n=1}^{\infty}\frac{4(n\pi)^4}{L_b^4}\delta_n^2\frac{L_b}{2} = \frac{E_s J_b}{L_b^3}\pi^4\sum_{n=1}^{\infty}n^4\delta_n^2 \tag{2}$$

where the explicit reference to functional dependence on location x is dropped. . For inelastic increments where the current tangent modulus is E_{st}, E_s is replaced by the reduced modulus E_r

$$E_r = 4E_s E_{st}\Big/\left(\sqrt{E_s}+\sqrt{E_{st}}\right)^2 \tag{3}$$

The second term in the strain energy equation is derived from the stretching in the uniform springs of linear stiffness $\beta_t = \alpha_t/s_t$. Noting that the stretch in a spring at a distance x is given by $y(x)$, the second term in the strain energy equation evaluates to

$$\Delta U_{ties} = \frac{\beta_t}{2}\int_0^{L_b} y^2\,dx = \frac{\beta_t}{2}\sum_{n=1}^{\infty}\delta_n^2\frac{3L_b}{8} = \frac{3\beta_t}{16}L_b\sum_{n=1}^{\infty}\delta_n^2 \tag{4}$$

Combining Eq. (2) and (4) leads to the following elastic strain energy ΔU_e,

$$\Delta U_e = \Delta U_{bar} + \Delta U_{ties} = \sum_{n=1}^{\infty}\frac{E_s J_b}{L_b^3}\left(n^2\pi^2\right)^2\delta_n^2 + \sum_{n=1}^{\infty}\frac{3\beta_t}{16}L_b\,\delta_n^2 \tag{5}$$

The external work done by P is evaluated by computing the change (shortening) in the bar length ΔL. The updated length is evaluated by integration along the deformed shape and can be evaluated using first-order expansion,

$$\Delta W = P\Delta L = P\int_0^{L_b}\left(\sqrt{1+\left(\frac{dy}{dx}\right)^2}-1\right)dx \approx \frac{P}{2}\int_0^{L_b}\left(\frac{dy}{dx}\right)^2 dx = \frac{P\pi^2}{4L_b}\sum_{n=1}^{\infty}\delta_n^2 \tag{6}$$

Equations (5) and (6) are derived using elastic material properties. However, unless the transverse reinforcement spacing is severely inadequate, longitudinal bar buckling often takes place after yielding. This can be addressed using incremental forms of Eq. (5) and (6). Hence, equating the expressions for internal and external work increments, substituting current material properties, and setting $n=1$ for the critical case, leads to the following non-monotonic relationship between the critical buckling load P_{cr} and the buckling length L_{cr},

$$P_{cr} = \frac{4\pi^2 E_r J_b}{L_{cr}^2}\left(1+\frac{3\beta_t L_{cr}^4}{16\pi^4 E_r J_b}\right) \tag{7}$$

which is minimized with respect to L_{cr} to find the minimum critical load $P_{cr,min}$ and the corresponding critical length $L_{cr,min}$.

$$L_{cr,min} = \left\{L_{cr} : \frac{\partial P_{cr}}{\partial L_{cr}} = \frac{-8\pi^2 E_r J_b}{L_{cr}^3} + \frac{3\beta_t L_{cr}}{2\pi^2} = 0\right\} = 2\pi\sqrt[4]{\frac{E_r J_b}{3\beta_t}} \geq s_t \tag{8}$$

$$P_{cr,min} = \left\{P_{cr} : L_{cr} = L_{cr,min}\right\} = \begin{cases} 8\pi^2 E_r J_b\big/L_{cr,min}^2 & \text{if} \quad L_{cr,min} > s_t \\ 4\pi^2 E_r J_b\big/s_t^2 & \text{if} \quad L_{cr,min} = s_t \end{cases} \tag{9}$$

The constraint $L_{cr} \geq s_t$ verifies the assumption that the tie spacing is such that buckling takes place over multiple ties. In the case of wider tie spacing, $L_{cr} < s_t$ is inadmissible and buckling is assumed to take place between two adjacent ties ($L_{cr,\min} = s_t$). In this case, the critical buckling load is corrected to exclude the effect of transverse tie stiffness, hence the discontinuity in Equation (9) at $L_{cr,\min} = s_t$. For a bar with cross-section area A_b, it is more convenient to evaluate a critical buckling stress (compression negative) at any stage during the analysis as

$$\sigma_{cr,\min} = \begin{cases} -2\sqrt{3\gamma_{cr}}\big/A_b & \text{if} \quad L_{cr,\min} > s_t \\ -4\pi^2 E_r J_b \big/ \left(A_b s_t^2\right) & \text{if} \quad L_{cr,\min} = s_t \end{cases} \tag{10}$$

where $\gamma_{cr} = E_r J_b \beta_t$ is a quantity that reflects the effect of inelasticity in the bar and transverse ties on the critical buckling stress. Inelasticity in the bar will reduce its stiffness modulus and buckling stress. Inelasticity or failure of the ties will result in a larger buckling length and a lower critical stress. Since inelasticity is a function of the imposed strain history, Eq. (10) therefore describes a critical surface in the bar stress-strain space which determines the onset of buckling. This critical surface is demonstrated in Fig.2 by evaluating $\sigma_{cr,\min}$ at axial strain increments, for a bar buckling over a single spacing, with yield stress σ_y and ultimate stress σ_u. Since the bar constitutive material model includes a yield plateau where the tangent modulus is zero, the critical surface definition uses the secant modulus during the perfectly plastic region.
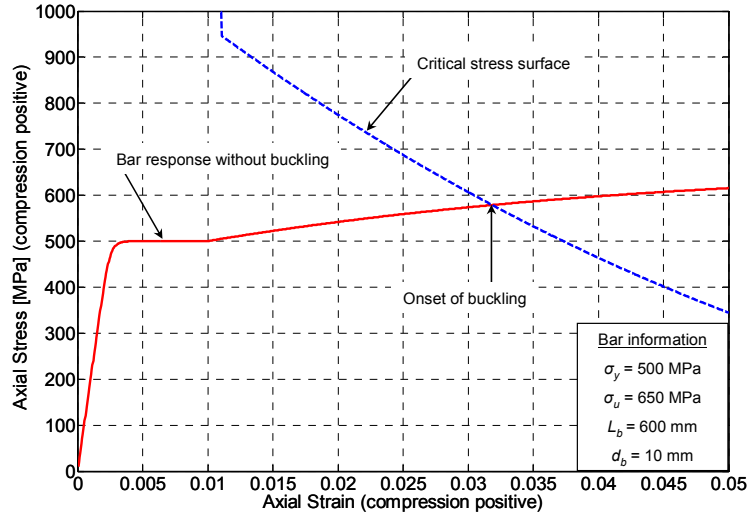
Figure 2. Onset of bar buckling and effect of bar inelasticity

Monotonic Post-Buckling Behavior

The mainstay of this model is its strain decomposition approach which enables the use of an existing steel stress-strain model as base. First, consider the linear-elastic behavior of a classic axially loaded steel bar with no lateral supports from transverse ties, and buckling length L_{cr} corresponding to a critical compressive stress $\sigma_{cr} = -4\pi^2 E J_b \big/ A_b L_{cr}^2$. The initial conditions of the bar correspond to stress-free ends. An initial imperfection is assumed that results in a mid-height

lateral deflection δ_i. The initial bowed profile $y_i(x)$ is described by Eq.(1), with δ_n replaced by δ_i. Hence, the shortest distance between the ends of the bar is smaller than the full length, which is interpreted as an initial shortening corresponding to initial stress-free strain ε_{fi},

$$\varepsilon_{fi} = \frac{\Delta L_i}{L_{cr}} = -\frac{1}{L_{cr}} \int_0^{L_{cr}} \left(\sqrt{1 + \left(\frac{dy}{dx}\right)^2} - 1 \right) dx \approx -\frac{1}{L_{cr}} \int_0^{L_{cr}} \frac{1}{2}\left(\frac{dy}{dx}\right)^2 dx = -\frac{\pi^2 \delta_i^2}{4L_{cr}^2} \qquad (11)$$

When the bar is loaded with an axial load P, the resulting deflected profile $y(x)$ is the algebraic sum of a profile $y_1(x)$ obtained from the general second-order equilibrium solution of a beam with fixed ends and the particular solution representing the initial profile, $y_i(x)$.

$$y_1(x) = \frac{1}{\left(4\pi^2/k_b^2 L_{cr}^2 - 1\right)} \frac{\delta_i}{2}\left[1 - \cos\left(\frac{2\pi}{L_{cr}} x\right)\right] \qquad (12)$$

where $k_b^2 = P/EJ_b$. Next, define the ratio α_P such that

$$\alpha_P = \frac{\sigma}{\sigma_{cr}} = \frac{P}{4\pi^2 EJ_b/L_{cr}^2} = k_b^2 L_{cr}^2/4\pi^2 \qquad (13)$$

and substitute in Eq. (12), and then add $y_i(x)$ to obtain

$$y(x) = y_i(x) + y_1(x) = \frac{\delta_i}{2}\left[1 - \cos\left(\frac{2\pi}{L_{cr}} x\right)\right] \frac{1}{(1 - \alpha_P)} = \frac{y_i(x)}{(1 - \alpha_P)} \qquad (14)$$

The physical significance of the previous derivation represents an interesting concept. An applied stress on the bar σ results in amplification of the bowed initial shape by a factor dependant on the ratio $\alpha_P = \sigma/\sigma_{cr}$. As a result, the total strain ε_t along the buckling length of the bar comprises two components: the stress-inducing mechanical strain ε_s in the steel material and an additional stress-free shortening ε_f due to amplification of the initial imperfection. In the linear elastic range, the first term is dominant, and can typically be computed as $\varepsilon_s = \sigma/E_s$. The second term is computed by making use of Eqs. (11) and (14),

$$\varepsilon_t = \varepsilon_s + \varepsilon_f \quad \text{and} \quad \varepsilon_f = \varepsilon_{fi}/(1 - \alpha_P)^2 \qquad (15)$$

Given the small typical values of α_p in the elastic range and the small common values for initial imperfection, the value of ε_f is insignificant prior to buckling or yielding in compression and can be neglected in estimating the linear response without any notable loss of accuracy. However, yielding or buckling of the bar significantly changes its stiffness and alters the value of α_P. Hence, when the bar reaches either limit case, the bar structural system is redefined according to the new material constants, and the initial boundary conditions are set to the current configuration of the loaded bar with its current deflection profile. Consider the case of a bar which has reached its yielding strain and is starting to exhibit hardening behavior. The "new" initial conditions are at the yield point in compression $\left(-\sigma_y, -\varepsilon_y = -\sigma_y/E_s\right)$, with the

stress-free strain computed per Eq. (15). These initial conditions are listed with a superscript h to denote that loading is taking place in the hardening phase,

$$\sigma_i^h = -\sigma_y \quad \text{and} \quad \varepsilon_{fi}^h = -\varepsilon_y + \varepsilon_{fi}\big/\left(1 - \sigma_y/\sigma_{cr}\right)^2 \approx -\varepsilon_y \tag{16}$$

The approximation in Equation (16) is valid since the stress-free strain can be ignored in the elastic range. This has the advantage of eliminating the model's sensitivity to the estimated value of δ_i. Next, the strain relationships of Eq. (15) are re-written using the new boundary conditions,

$$\varepsilon_t = \left(\varepsilon_s - \varepsilon_{fi}^h\right) + \varepsilon_f^h \quad \text{and} \quad \varepsilon_f^h = \varepsilon_{fi}^h \big/ \left(1 - \alpha_{\Delta P}^h\right)^2 \tag{17}$$

where $\alpha_{\Delta P}^h$ is a redefinition of the ratio α_P according to

$$\alpha_{\Delta P}^h = \left(\sigma(\varepsilon_s) - \sigma_i^h\right)\big/\left(\sigma_{cr}^h - \sigma_i^h\right) \geq 0 \tag{18}$$

where $\sigma(\varepsilon_s)$ represents the constitutive law of the base model and the updated critical stress σ_{cr}^h is computed using Eq. (10) and the reduced stiffness modulus. Eqs. (17) and (18) can be satisfied using an iterative solver. Note that ε_t and ε_s represent the total and mechanical strains in the bar and are not affected by the hardening regime, hence the absence of superscript h. If the updated critical stress σ_{cr}^h is lower than the yield stress and the bar therefore buckles before hardening, the bar base material effectively unloads while the observed (total) strain increases. Otherwise, the stress in the bar will continue to increase until it reaches the buckling stress, yet the bar's stress-total strain response will exhibit reduced hardening stiffness due to the decomposition of total strain between a mechanical component that generates stress and a stress-free component.
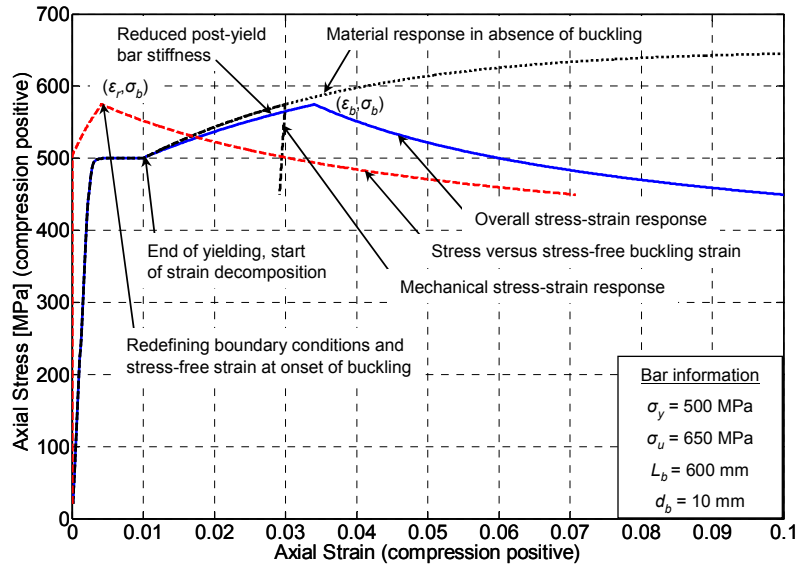
Figure 3. Model illustration of monotonic post-buckling behavior

Finally, when bar buckling is detected by Eq. (10), another redefinition of the boundary conditions is imposed to update Eqs. (17) and (18), with superscript b for the buckling phase:

$$\varepsilon_t = \left(\varepsilon_s - \varepsilon_b\right) + \varepsilon_f^b \quad \text{and} \quad \varepsilon_f^b = \varepsilon_r + \varepsilon_b\big/\left(1 - \alpha_{\Delta P}^b\right)^2 \tag{19}$$

$$\alpha_{\Delta P}^{b} = \left(\sigma(\varepsilon_s) - \sigma_b\right)\big/\left(\sigma_{cr|\infty} - \sigma_b\right) \geq 0 \qquad (20)$$

where (σ_b, ε_b) is the base material's stress and strain at buckling, $\sigma_{cr|\infty}$ is the lowest asymptotic critical stress calculated by Eq. (10) for the critical surface at the highest credible strain level, and the residual strain term ε_r preserves strain compatibility in the decomposition equation. This residual strain is equal to the stress-free strain ε_f^h (if any) at the onset of buckling. The main components and behavioral features of this model are illustrated in Fig.3. The base stress-strain model for the bar is assumed to follow (Chang and Mander 1994).

Cyclic Post-Buckling Behavior

The cyclic response modification to the base stress-strain model involves the following: (1) reduction of the unloading stiffness after a compression cycle in which buckling occurred due to straightening of the bar (Dhakal and Maekawa 2002b); (2) tracking of the gradual tension stiffening behavior in the straightening bar as the stress-free strain is recovered; (3) accounting for the amount of this straightening in calculating the reduced buckling stress during subsequent compression cycles; and (4) hysteretic reduction in stress up to bar fracture (Brown and Kunnath 2004). The details of this model are documented in (Talaat and Mosalam, 2007).

Numerical Simulations of Bar Buckling Tests

The proposed model is compared to experimental results published in (Monti and Nuti 1992), (Rodriguez et al. 1999), and (Bae et al. 2005) to assess its validity. The simulated experimental investigations include individual steel bars subjected to monotonically increasing compressive strains or cyclically increasing strain levels. The end conditions for all bars are prevented from rotation and lateral translation. The stress-strain parameter values used in the analytical simulation for each group of experiments are listed in Table 1 and defined in Fig.4.a. Analytical simulation is performed using the developed bar buckling model and a base stress-strain material model for the reinforcing steel. The base stress-strain model in (Chang and Mander 1994) is used, except for simulations of (Monti and Nuti 1992) where (Menegotto and Pinto 1973) is used due to unreported parameter values (Table 1).

Table 1. Parameter values in bar buckling simulations

Experiment	(Bae et al. 2005)	(Rodriguez et al. 1999)	(Monti and Nuti 1992)
E_s [GPa]	200	200	200
E_{sh} [GPa]	5	10	8
σ_y [MPa]	440	409	490
σ_u [MPa]	640	700	Not Available
ε_{sh}	0.005	0.005	Not Available
ε_u	0.16	0.18	Not Available

Fig.4.b shows the comparison between the model predictions and the monotonic compression tests reported in (Bae et al. 2005) for nine levels of the bar slenderness ratio $L_b/d_b = 4,5,...,12$. The simulation is successful in capturing the buckling stress for the majority

of bars except for bars which buckle prior to yielding, with slenderness ratio $L_b/d_b \geq 10$. The critical buckling surface during the yielding plateau is not well defined as previously discussed. The model is reasonably successful in reproducing the reduction in hardening stiffness between yielding and buckling. The model is generally successful in describing the post-buckling softening in the bars. The analytically simulated softening branches show discontinuity and steeper gradients occurring at lower strains at the onset of buckling. This cannot be observed in the experiments due to the load control approach and the average strain calculation method.

(a) Bar stress-strain model parameters   (b) Model comparisons to experimental results
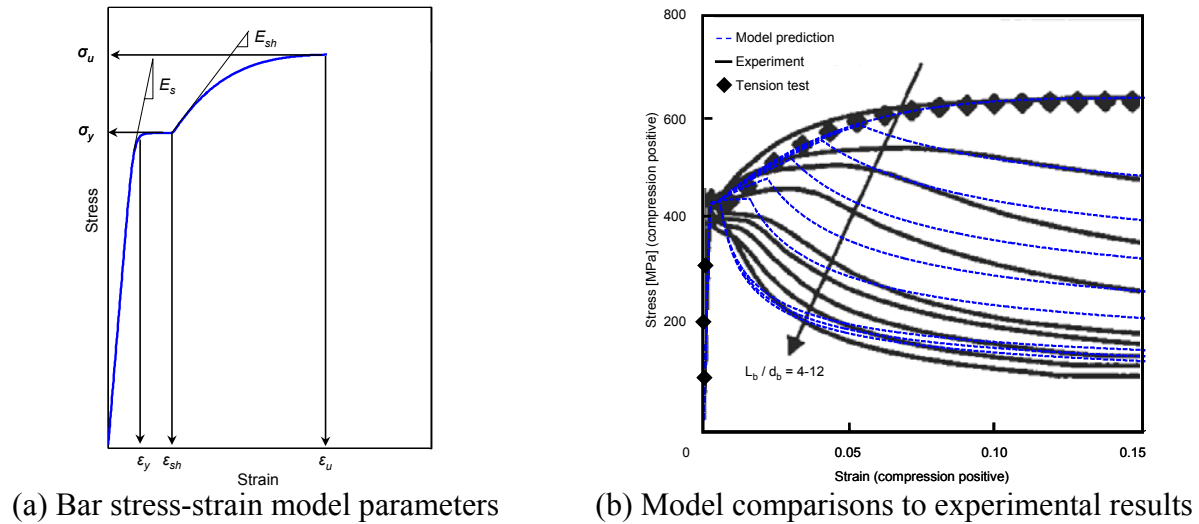
Figure 4. Model simulations of (Bae et al. 2005) bar buckling experiments

Fig.5.a shows the comparison between the model prediction and the cyclic loading experiments conducted in (Rodriguez et al. 1999) for a bar representing the compression (concave) side of an axially loaded RC column subjected to cyclic lateral displacement. The simulated behavior compares well with the experiment over multiple cycles where buckling-induced softening is observed. The area of the hysteretic loops in tension after unloading from large compression strain levels is only slightly larger in the simulations.

Fig.5.b shows the comparison between the model prediction and the cyclic loading tests conducted in (Monti and Nuti 1992) for steel bars with slenderness ratios of 11. The base material response of the latter steel bars follows the stress-strain model in (Menegotto and Pinto 1973) due to the limited material properties reported in the test. The simulations are generally successful in estimating the cycles where buckling is observed and the subsequent softening in stress, in estimating the reduced stiffness moduli of the buckled bars upon unloading from compression, and in reproducing the subsequent hysteretic behavior in tension. The area of the hysteretic loops in compression is underestimated in the simulation at large strain magnitudes in Fig.5.b due to the limitations of the base stress-strain model. This is demonstrated in the super-imposed response using the same base stress-strain model without buckling (Dhakal and Maekawa 2002b). The comparison highlights the contribution of the developed bar buckling model. This discrepancy only appears for highly slender bars and can be calibrated in the presence of additional data and more refined base stress-strain models. The simulated bar buckling response at slenderness ratios of 8 and 5 (not shown) do not exhibit this difference in hysteretic loop area.

(a) $L_b/d_b = 6$, (Rodriguez et al. 1999)   (b) $L_b/d_b = 11$, (Monti and Nuti 1992)
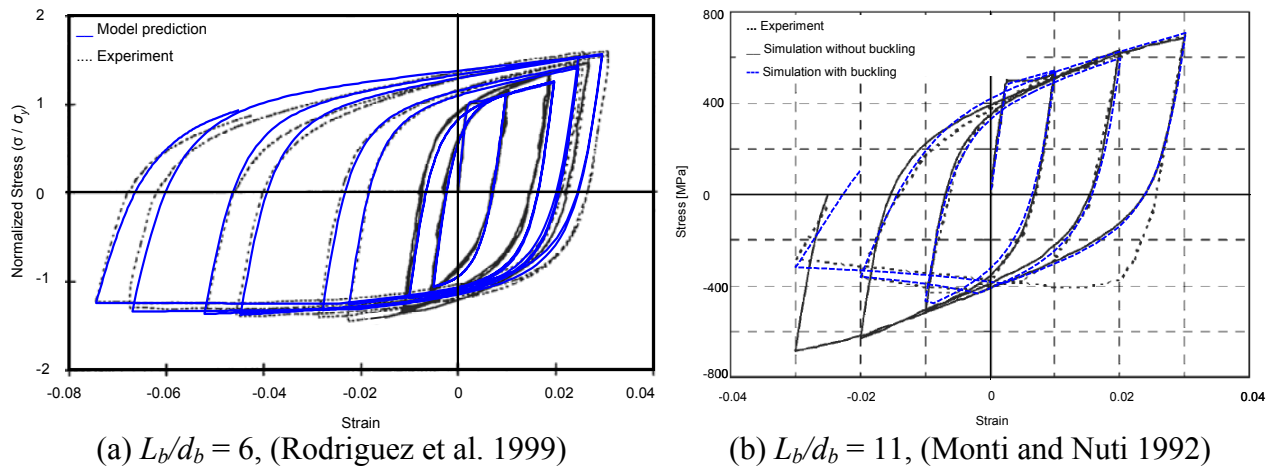
Figure 5. Model simulations of cyclic bar buckling experiments

Numerical Simulation of RC Column Tests

Both column specimens investigated in (Henry 1998) have identical dimensions and longitudinal reinforcement. Each column is 610 mm in diameter and 2440 mm in length, in addition to a RC anchor block of approximately 730 mm thickness. Column longitudinal reinforcement consists of 22 steel bars of 16 mm diameter distributed uniformly around the circular cross-section and anchored by extending them inside the anchor block while their ends are terminated with 90° bents. Transverse reinforcement consists of 6.4 mm spirals pitched at a spacing prescribed for each specimen along the entire column. A fixed axial load is applied on each specimen using two steel rods post-tensioned against a steel beam positioned at the top of the column, which nearly eliminates P-Δ effects. Symmetric cycles of increasing amplitude of lateral displacements are applied using a displacement-controlled actuator with three repetitions at each displacement level. The lateral displacement and the applied lateral load at the column tip are measured. The axial strain at seven locations along three longitudinal bars is recorded using electrical strain gauges. Specimen designations are:

1. 415P: Axial load = 1310 kN (20% $f'_c A_g$), transverse spiral pitch = 32 mm,
2. 415S: Axial load = 655 kN (10% $f'_c A_g$), transverse spiral pitch = 64 mm.

The FE model of each column consists of a force-based lumped-plasticity beam-column element. No P-Δ effect is included in the stiffness matrix. The end plastic hinges are defined using the confined cross-section model and the confined concrete uniaxial fiber model developed in (Mosalam et al., 2007), with 18 and 2 uniform-thickness layers used to discretize the cross-section within the core and cover regions, respectively (Fig.6.a). Each layer is segmented into 18 circumferential sectors encircling a 20° central angle. The fibers representing the steel bars are modeled using the bar buckling model, with the material model in (Menegotto and Pinto 1973) as the base mechanical stress-strain relationship. The plastic hinge length is adopted from the measured lengths over which longitudinal reinforcement is recorded to have yielded. These lengths are reported in (Henry 1998) to be 765 and 612 mm for specimens 415P and 415S, respectively. The flexibility of the elastic segment of the column is computed using half of the

concrete elastic modulus to account for the effect of flexural cracking. The effect of yield penetration is modeled using a calibrated rotational spring model (Alsiwat and Saatcioglu, 1992).

The confined cross-section model in (Mosalam et al., 2007) enables the determination of the stress-state in the spiral reinforcement using quasi-lateral strain compatibility. Since this model is currently validated only for monotonic curvature increments, the constructed FE models are subjected to the imposed axial load and then to simulated pushover by imposing increasing lateral deformation at the column tip. For comparison and assessment of model performance, a second set of pushover analyses is constructed using the same structural models while disabling the buckling feature of the longitudinal steel bars. The comparison is shown in Fig.6.b for specimen 415S (results for specimen 415P are similar). Both simulated pushover curves agree well with the initial stiffness, the yield displacement, and the envelope of the pre-peak cyclic response. The buckling-enabled FE model successfully identifies first bar buckling at a lateral displacement of 5.08 in., corresponding to the displacement level at which first bar buckling is observed, and is capable of generally following the rapidly descending branch of the envelope, while the buckling-disabled FE model is not. FE simulation of the hysteretic column behavior and effects of stress reduction is currently underway.

(a) FE model discretization   (b) Specimen 415S force-displacement response
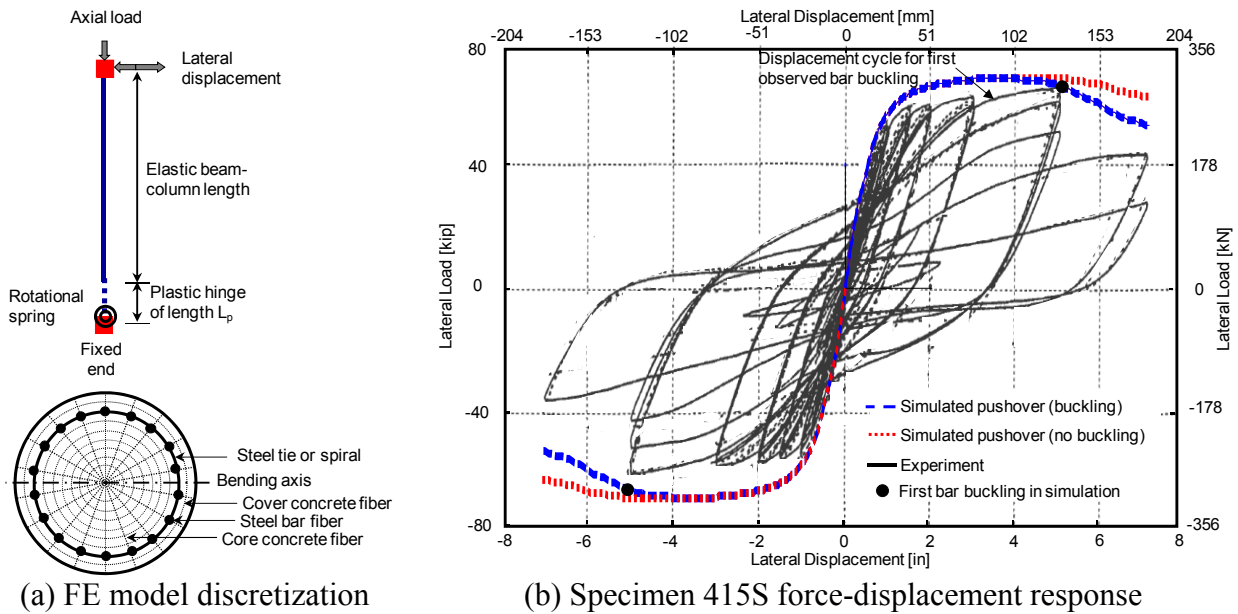
Figure 6. Numerical simulation of RC column tests in (Henry 1998)

Conclusions

This paper presents a constitutive model for longitudinal steel bars in RC columns, laterally restrained by transverse reinforcement (ties), which achieves the following:

1. Determines the compressive stress at bar buckling, incorporating tie stiffness;
2. Uses a strain decomposition approach with an existing steel stress-strain base model;
3. Capture the post-yield reduction in stiffness and the post-buckling softening response;
4. Accounts for the decrease in stiffness in the tension response of buckled bars;

5. Incorporates hysteretic stress reduction;

6. Compares well with several experimental bar buckling tests.

7. One major advantage of the developed bar buckling model is its flexibility for use with existing libraries of steel material base models. Clearly, the accuracy of the results will depend on how refined the base model is and, particularly, how accurately it represents the changes in bar stiffness.

8. The developed bar buckling model was used in FE models of RC columns subjected to lateral load. The simulated push-over response compared well with the envelope of the experimental cyclic response, identified the onset of bar buckling, and matched the post-peak drop in lateral capacity.

Acknowledgment

References

Alsiwat, J.M. and Saatcioglu, M. (1992). Reinforcement Anchorage Slip under Monotonic Loading. *ASCE Journal of Structural Engineering* 118(9): 2421-2438.

Attolico, A., Biondi, S., Nuti, C. and Petrangeli, M. (2000). Influence of Buckling of Longitudinal Rebars in Finite Element Modeling of Concrete Structures Subjected to Cyclic Loading. *12th World Conference on Earthquake Engineering, Auckland, New Zealand*.

Bae, S., Mieses, A.M. and Bayrak, O. (2005). Inelastic Buckling of Reinforcing Bars. *ASCE Journal of Structural Engineering* 131(2): 314-321.

Bayrak, O. and Sheikh, S.A. (2001). Plastic Hinge Analysis. *ASCE Journal of Structural Engineering* 127(9): 1092-1100.

Berry, M.P. and Eberhard, M.O. (2005). Practical Performance Model for Bar Buckling. *ASCE Journal of Structural Engineering* 131(7): 1060-1070.

Brown, J. and Kunnath, S.K. (2004). Low-Cycle Fatigue Failure of Reinforcing Steel Bars. *ACI Materials Journal* 101(6): 457-466.

Dhakal, R.P. and Maekawa, K. (2002a). Reinforcement Stability and Fracture of Cover Concrete in Reinforced Concrete Members *ASCE Journal of Structural Engineering* 128(10): 1253-1262.

Dhakal, R.P. and Maekawa, K. (2002b). Path-Dependent Cyclic Stress-Strain Relationship of Reinforcing Bar Including Buckling. *Engineering Structures* 24(11): 1383-1396.

Gomes, A. and Appleton, J. (1997). Nonlinear Cyclic Stress-Strain Relationship of Reinforcing Bars Including Buckling. *Engineering Structures* 19(10): 822-826.

Henry, L. (1998). *Study of Buckling of Longitudinal Bars in Reinforced Concrete Bridge Columns*. MS Thesis, University of California, Berkeley.

Menegotto, M. and Pinto, P. (1973). Method of Analysis for Cyclically Loaded Reinforced Concrete Plane Frames Including Changes in Geometry and Non-Elastic Behavior of Elements under Combined Normal Force and Bending. *Symposium on Resistance and Ultimate Deformability of Structures Acted on by Well Defined Repeated Loads*, IABSE: 13, 15-22.

Mosalam, K.M., Talaat, M. and Binici, B. (2007). A Computational Model for Reinforced Concrete Members Confined with Fiber Reinforced Polymer Lamina: Implementation and Experimental Validation. *Composites Part B: Engineering* 38(5-6): 598-613.

Rodriguez, M.E., Botero, J.C. and Villa, J. (1999). Cyclic Stress-Strain Behavior of Reinforcing Steel Including Effect of Buckling. *ASCE Journal of Structural Engineering* 125(6): 605-612.

Talaat, M., and Mosalam, K.M. (2007). *Computational Modeling of Progressive Collapse in Reinforced Concrete Frame Structures*. PEER Technical Report 2007/10.